1 Supplement of

2 Contrasting Impacts of Dust Ice-Nucleating Particles on the

3 Evolution and Radiative Effects of Mixed-Phase and Ice Clouds

- 4 Hua Zhang et al.
 - Correspondence: Bin Zhao (bzhao@mail.tsinghua.edu.cn)

Text S1. Default Morrison microphysics scheme

In WRF-Chem, the default Morrison microphysics scheme is a two-moment bulk stratiform cloud microphysics scheme that traces the number concentrations and mass mixing ratios of five water condensates: ice crystals, graupel, snow, cloud droplets, and rain, and treats several microphysical processes: hydrometer collection, condensation/evaporation, freezing, melting, sedimentation, and ice nucleation Morrison and Gettelman (2008).

Within the default Morrison microphysics scheme, these heterogeneous nucleation pathways are parameterized separately. At temperatures below -4° C, both immersion and contact freezing can be activated. Immersion freezing follows the classical parameterization of Bigg (1953). Contact freezing is represented through the flux of contact nuclei to droplets via Brownian motion, diffusion electrophoresis, and thermophoresis, with effective diffusion coefficients provided by Young (1974). The number concentration of contact nuclei is calculated following Meyers et al. (1992). According to Cooper (1986), deposition nucleation becomes active when the temperature is below -8° C and the saturation ratio with respect to water exceeds 0.999 (Cooper, 1986). However, because the Cooper's parameterization produces unrealistically high INP number concentrations at colder temperatures, the Morrison microphysics scheme imposes an upper limit of 500 L⁻¹ on the INP number concentration for deposition nucleation.

To ensure physical consistency, the scheme further constrains the number of ice crystals generated by immersion and contact freezing so that they cannot exceed the number of available cloud droplets. Homogeneous freezing is assumed to occur spontaneously for cloud droplets and raindrops at temperatures below -40° C (Morrison et al., 2005). In addition, secondary ice formation is incorporated through the Hallett–Mossop rime-splintering mechanism (Hallett and Mossop, 1974).

Text S2. Cubic interpolation function $\delta_a^b[y, y_1, y_2]$

36
$$\delta_a^b = \begin{cases} a, & (y \le y_1) \\ b, & (y \ge y_2) \\ a_0 + a_1 y + a_2 y^2 + a_3 y^3, & (y_1 < y < y_2) \end{cases}$$
 (S1)

37 where $a_0 = B$, $a_1 = Ay_1y_2$, $a_2 = -A(y_1 + y_2)/2$, $a_3 = A/3$, $A = 6(a - b)/(y_2 - y_1)^3$, and 38 $B = a + Ay_1^3/6 - Ay_1^2y_2/2$.

Table S1. Parameters of the ice nucleation parameterization in Reicher et al. (2019).

Diameter	Parameters	Valid temperature
range		range
0.3–1 μm	$y_0 = 9.48, a = 23.00, b = 1.34, c = 7.38$	238–266 K
1–10 μm	$y_0 = 11.4, a = 24.00, b = 1.53, c = 4.54$	236–266 K

Table S2. Parameters of the ice nucleation parameterization in Chen et al. (2021).

Diameter range	Parameters	Valid temperature range
0.18–1 μm	a = -0.480, b = 5.296	from -35°C to -10°C
1–1.8 μm	a = -0.423, b = 9.390	from -35 °C to -6 °C
1.8–3.2 μm	a = -0.425, b = 9.506	from -35° C to -6° C
3.2–5.6 μm	a = -0.428, b = 9.592	from -35 °C to -6 °C
5.6–10 μm	a = -0.441, b = 10.635	from -35 °C to -6 °C

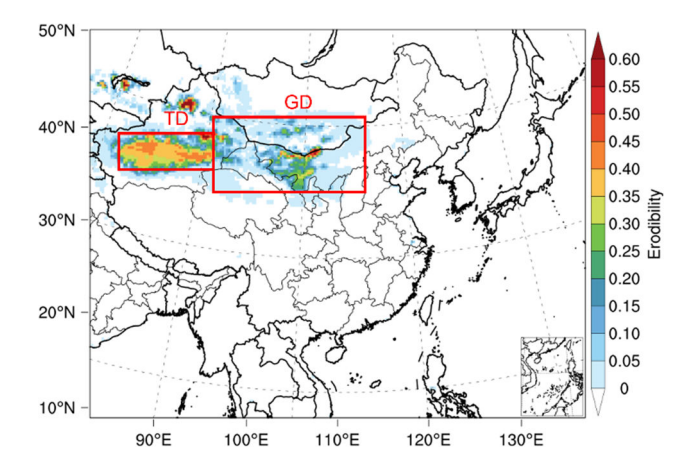


Figure S1. Model domain for the numerical simulations. The color shading represents the erodibility factor, defined as the fraction of erodible surface in each grid cell. TD refers to the Taklimakan Desert, and GD refers to the Gobi Desert.

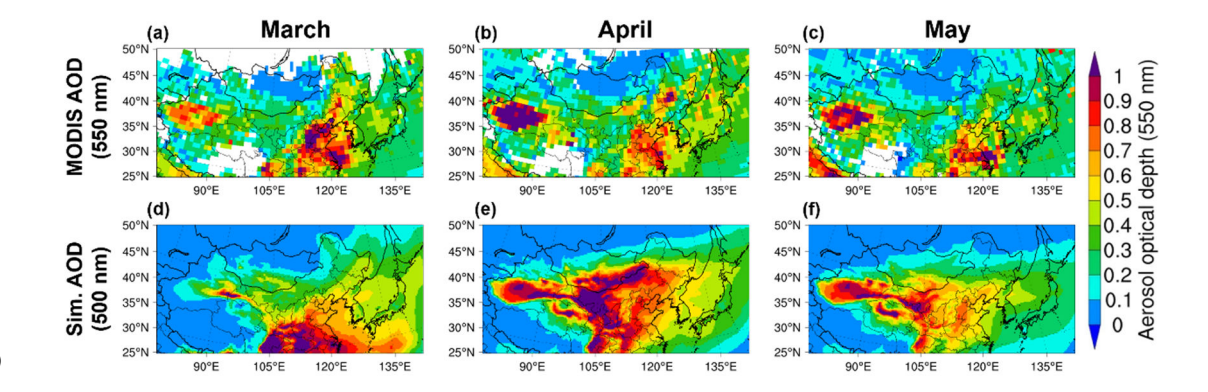


Figure S2. Comparison between simulated and observed aerosol optical depth (AOD) at the wavelength of 550 nm in March (left column), April (middle column), and May 2018 (right column). Panels (a-c) show AOD observations from MODIS, and panels (d-f) present the corresponding simulated AOD. The simulated results are from the MixIceINPs scenario and represent averages of hourly values.

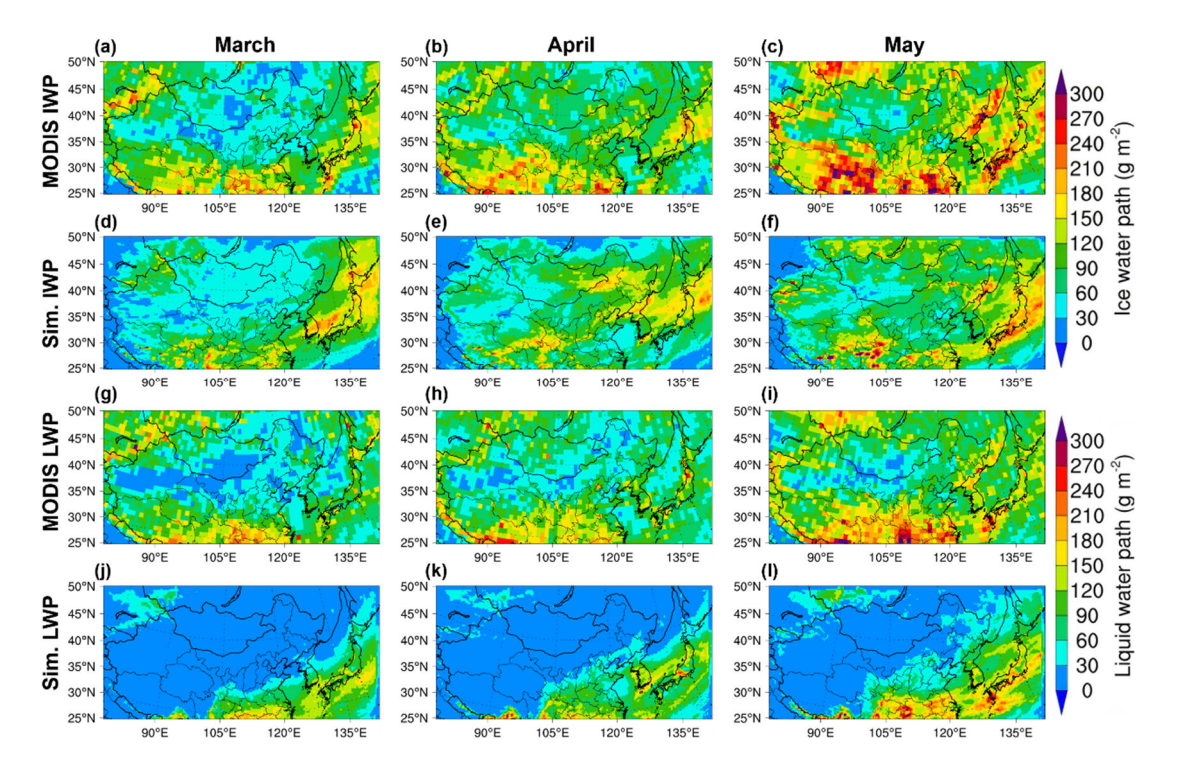


Figure S3. Comparison between simulated and observed ice water path (IWP) and liquid water path (LWP) in March (left column), April (middle column), and May 2018 (right column). Panels (a-c) show IWP observations from MODIS, and panels (d-f) present the corresponding simulated IWP. Panels (g-i) display LWP observations from MODIS, and panels (j-l) show the corresponding simulated LWP. The simulated results are from the MixIceINPs scenario and represent averages of hourly values.

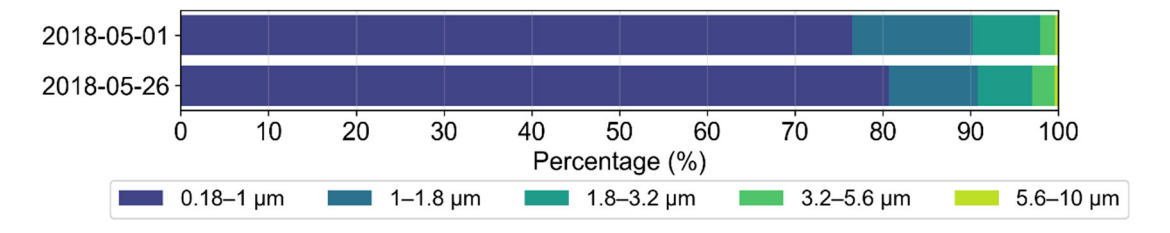


Figure S4. Simulated percentage contributions of different particle size bins (0.18–1 μm, 1–1.8 μm, 1.8–3.2 μm, 3.2–5.6 μm, and 5.6–10 μm) to the total dust surface area concentration (0.18–10 μm) on 1 and 26 May 2018 at the Peking University Atmospheric Environment Monitoring Station (116.31° E, 39.99° N). The simulated results are from the MixIceINPs scenario and represent averages of hourly values.



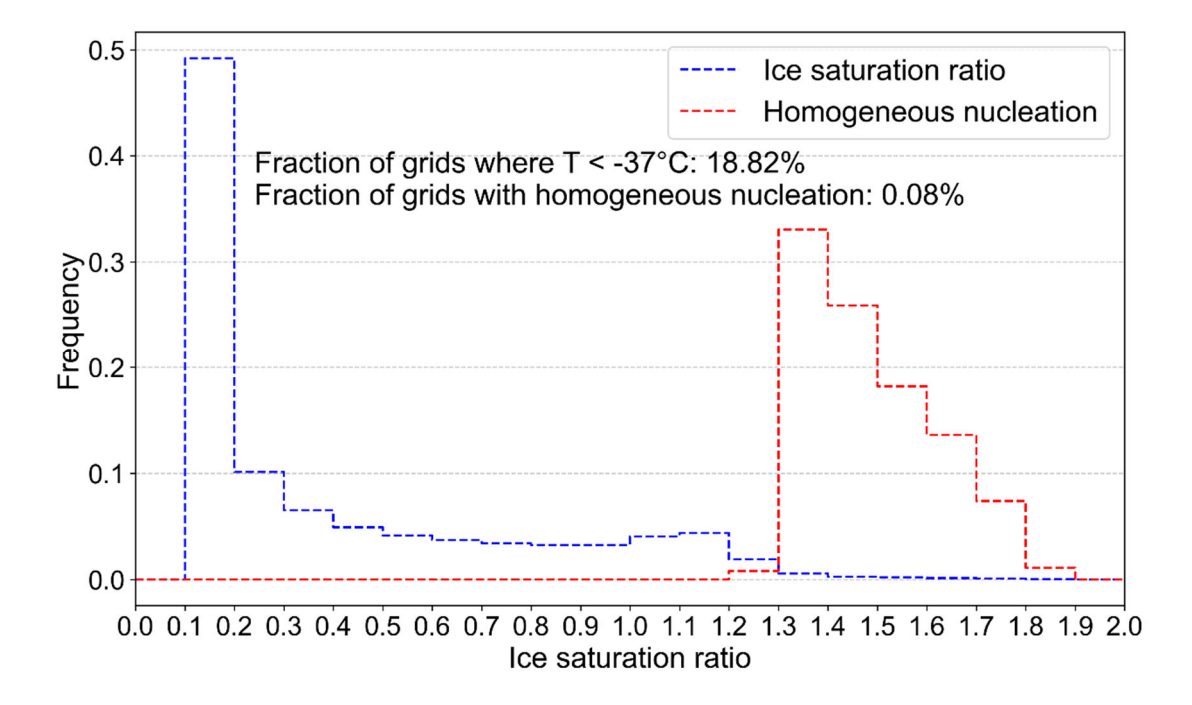


Figure S5. Simulated frequencies of ice saturation ratio and homogeneous nucleation occurrence as a function of ice saturation ratio. The statistics are derived from all hourly grid cells from March to May 2018 with temperatures below −37°C, which account for 18.82% of the total domain (as homogeneous nucleation can only occur under such conditions). For each ice saturation ratio interval, both the frequency of grid cells and the frequency of those undergoing homogeneous nucleation are calculated. Grid cells with ice saturation ratios greater than 1.3 (the interval where homogeneous nucleation primarily occurs) constitute less than 0.7% of the cold-grid subset (i.e., < 0.13% of the total domain), while those experiencing homogeneous nucleation represent less than 0.08% of the total domain. The simulated results are from the NoINPs scenario.

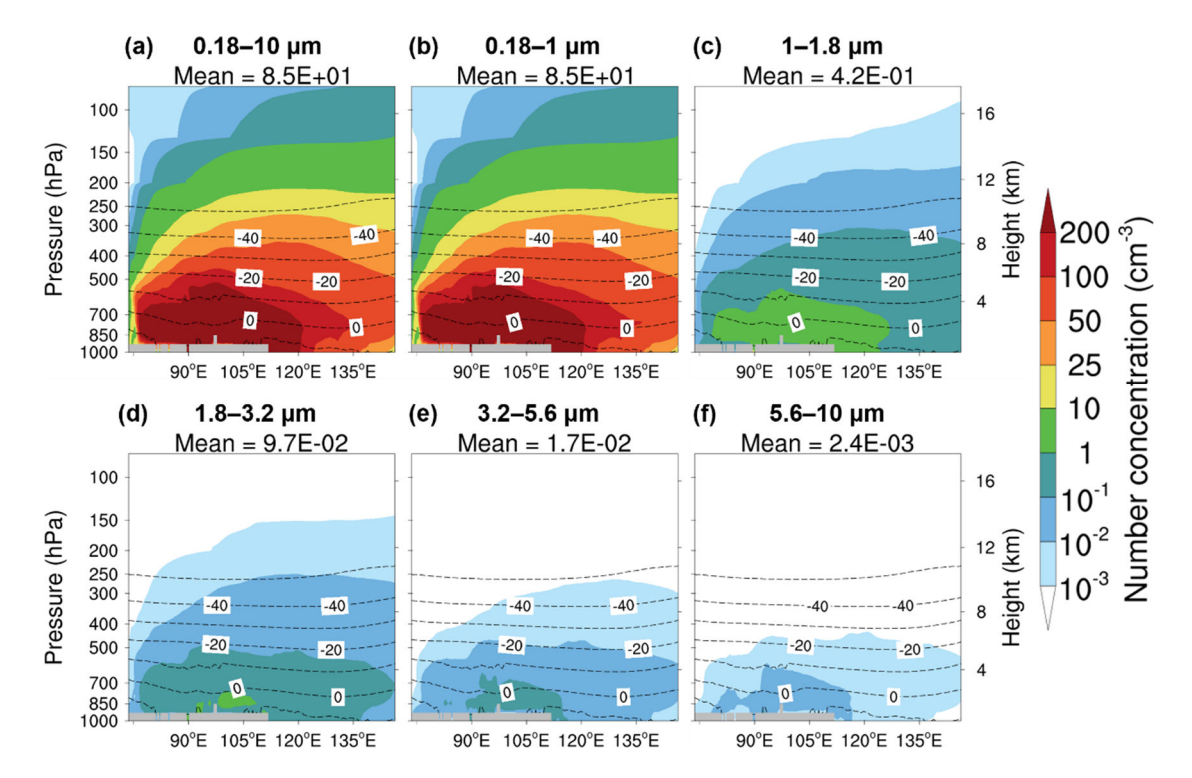


Figure S6. Simulated meridional mean vertical cross-sections of dust number concentrations for different particle size bins: (a) $0.18-10~\mu m$, (b) $0.18-1~\mu m$, (c) $1-1.8~\mu m$, (d) $1.8-3.2~\mu m$, (e) $3.2-5.6~\mu m$, and (f) $5.6-10~\mu m$. Dashed lines indicate isotherms, and grey shading denotes missing values due to terrain. The mean value over the plotted region is shown above each panel. The simulated results are from the MixIceINPs scenario and represent averages of hourly values from March to May 2018.

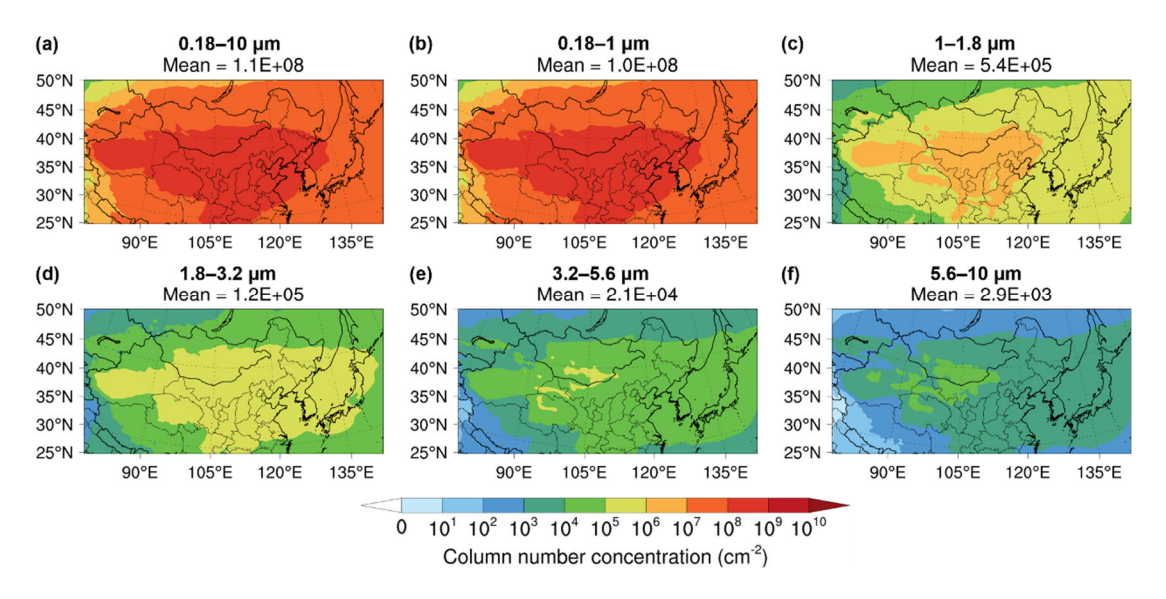


Figure S7. Simulated spatial distributions of dust column number concentrations (vertically integrated) for different particle size bins: (a) $0.18-10~\mu m$, (b) $0.18-1~\mu m$, (c) $1-1.8~\mu m$, (d) $1.8-3.2~\mu m$, (e) $3.2-5.6~\mu m$, and (f) $5.6-10~\mu m$. The mean value over the plotted region is shown above each panel. The simulated results are from the MixIceINPs scenario and represent averages of hourly values from March to May 2018.



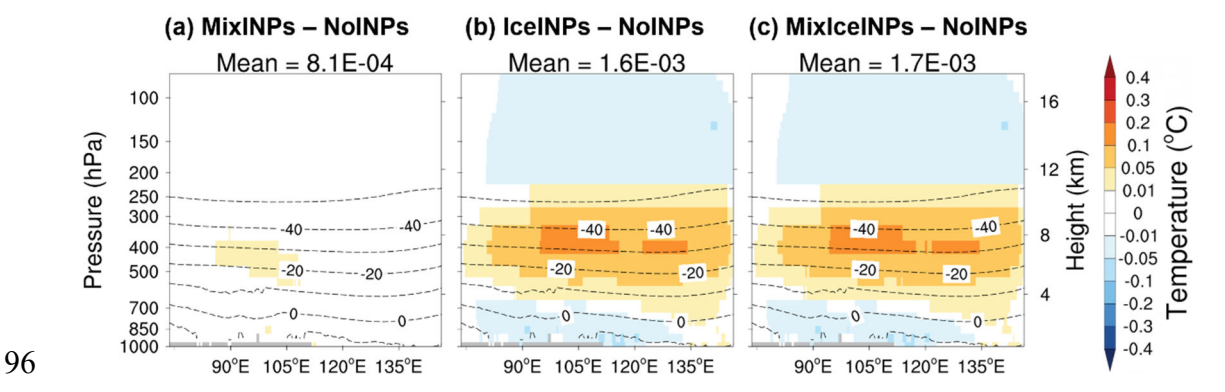


Figure S8. Simulated meridional mean vertical cross-sections of temperature differences: (a) MixINPs – NoINPs, (b) IceINPs – NoINPs, and (c) MixIceINPs – NoINPs. Dashed lines indicate isotherms, and grey shading denotes missing values due to terrain. The mean value over the plotted region is shown above each panel. The simulated results are averages of hourly values from March to May 2018.

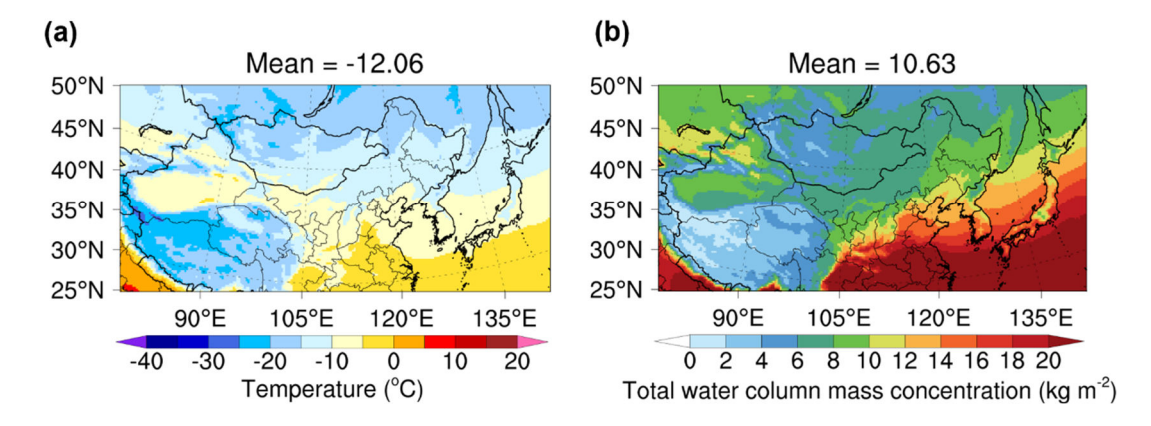


Figure S9. Simulated spatial distributions of (a) vertically averaged temperature and (b) vertically integrated total water column mass concentrations (sum of vapor, liquid, and ice). The mean value over the plotted region is shown above each panel. The simulated results are from the MixIceINPs scenario and represent averages of hourly values from March to May 2018.

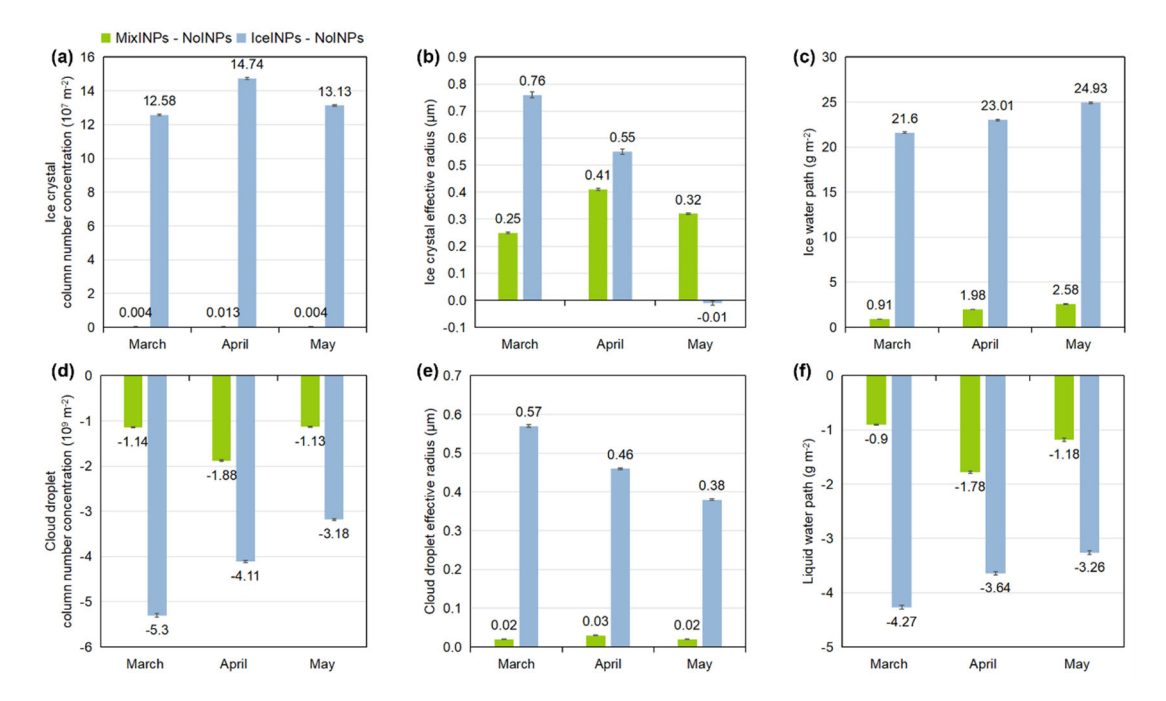


Figure S10. Simulated horizontal spatial means of (a) ice crystal column number concentration, (b) ice crystal effective radius, (c) ice water path, (d) cloud droplet column number concentration, (e) cloud droplet effective radius, and (f) liquid water path in March, April, and May 2018. The green bars denote the simulation results for the MixINPs – NoINPs scenario, while the blue bars denote those for the IceINPs – NoINPs scenario. Error bars denote the standard error of the mean (σ/\sqrt{N}) across grids, where σ is the standard deviation and N is the number of grids. The simulated results are monthly averages of hourly values.

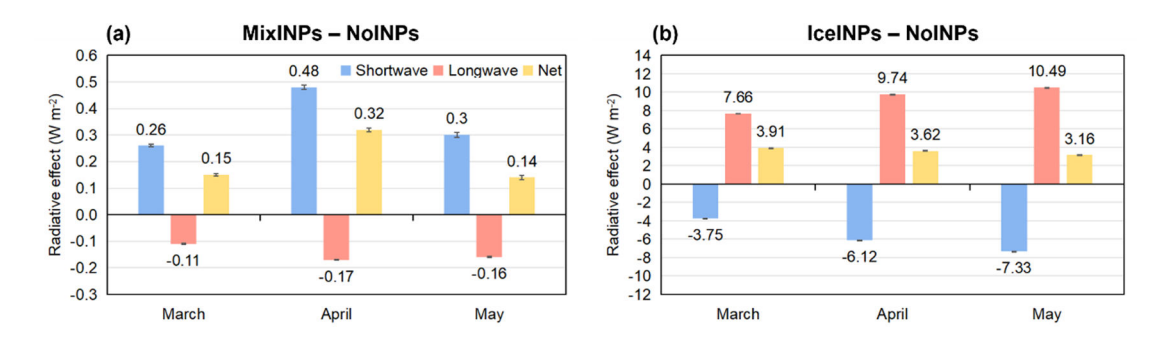


Figure S11. Simulated horizontal spatial means of the radiative effect of (a) INPs in mixed-phase clouds and (b) INPs in ice clouds in March, April, and May 2018. The blue bars denote shortwave radiation, the red bars denote longwave radiation, and the yellow bars denote net radiation. The error bars denote the standard error of the mean (σ/\sqrt{N}) across grids, where σ is the standard deviation and N is the number of grids. The simulated results are monthly averages of hourly values.

Reference

Bigg, E. K.: The formation of atmospheric ice crystals by the freezing of droplets, Q. J. R. Meteorolog. Soc., 79, 510–519, https://doi.org/10.1002/qj.49707934207, 1953.

- 128 Chen, K., Yin, Y., Liu, S., Liu, C., Wang, H., He, C., Jiang, H., and Chen, J.:
- 129 Concentration and variability of deposition-mode ice nucleating particles from
- Mt. Tai of China in the early summer, Atmos. Res., 253, 105426,
- https://doi.org/10.1016/j.atmosres.2020.105426, 2021.
- 132 Cooper, W. A.: Ice initiation in natural clouds, in: Precipitation Enhancement—A
- Scientific Challenge, American Meteorological Society, Boston, MA, 29–32,
- https://doi.org/10.1007/978-1-935704-17-1 4, 1986.
- Hallett, J. and Mossop, S. C.: Production of secondary ice particles during the riming
- process, Nature, 249, 26–28, https://doi.org/10.1038/249026a0, 1974.
- 137 Meyers, M. P., DeMott, P. J., and Cotton, W. R.: New primary ice-nucleation
- parameterizations in an explicit cloud model, J. Appl. Meteorol., 31, 708–721,
- https://doi.org/10.1175/1520-
- 140 0450(1992)031%253C0708:NPINPI%253E2.0.CO;2, 1992.
- 141 Morrison, H. and Gettelman, A.: A new two-moment bulk stratiform cloud
- microphysics scheme in the community atmosphere model, version 3 (CAM3).
- Part I: Description and numerical tests, J. Clim., 21, 3642-3659,
- 144 https://doi.org/10.1175/2008JCLI2105.1, 2008.
- 145 Morrison, H., Curry, J. A., and Khvorostyanov, V. I.: A new double-moment
- microphysics parameterization for application in cloud and climate models. Part
- 147 I: Description, J. Atmos. Sci., 62, 1665–1677, https://doi.org/10.1175/JAS3446.1,
- 148 2005.

- 149 Reicher, N., Budke, C., Eickhoff, L., Raveh-Rubin, S., Kaplan-Ashiri, I., Koop, T.,
- and Rudich, Y.: Size-dependent ice nucleation by airborne particles during dust
- events in the Eastern Mediterranean, Atmos. Chem. Phys., 19, 11143–11158,
- https://doi.org/10.5194/acp-19-11143-2019, 2019.
- Young, K. C.: The role of contact nucleation in ice phase initiation in clouds, J. Atmos.
- 154 Sci., 31, 768–776, https://doi.org/10.1175/1520-
- 155 0469(1974)031%253C0768:TROCNI%253E2.0.CO;2, 1974.